Hindawi
International Journal of Antennas and Propagation
Volume 2017, Article ID 9783541, 6 pages
https://doi.org/10.1155/2017/9783541

Research Article

Design and Simulation of an Antenna-Coupled Microbolometer at 30 THz

Angel Colin, Eduardo Pérez-Tijerina, and Francisco Solis-Pomar

Facultad de Ciencias Físico Matemáticas, Universidad Autónoma de Nuevo León, Av. Universidad s/n, Ciudad Universitaria, 66455 San Nicolás de los Garza, NL, Mexico

Correspondence should be addressed to Angel Colin; angel.colin@fcfm.uanl.mx

Received 27 April 2017; Accepted 28 May 2017; Published 3 July 2017

Academic Editor: Herve Aubert

We propose a model of antenna-coupled microbolometer to be included in an array for receiving and detecting long wave infrared (LWIR) electromagnetic radiation. The antenna is joined to microstrip bandpass filters thus forming a single metal structure to define the operation frequency band. The antenna and microstrip filters are modeled in aluminum thin film. The microbolometer is modeled with superconducting niobium, all together on a silicon nitride membrane. The squared pixel structure is designed on a support frame of 20 μm in size. Simulation results for this antenna exhibit a frequency range of operation from 27 to 35 THz and is configured for two arrays, one of 10×10 and the other one of 50×50 elements. The device has been simulated by means of the commercial electromagnetic software (HFSS), which is based on the finite elements method. The predicted values for the figures of merit of this microbolometer are as follows: $\tau = 5.8$ ns, $R_v = 5.3 \times 10^3$ V/W, and $D^* = 2.07 \times 10^{10}$ cm$\sqrt{\text{Hz}}$/W, respectively.

1. Introduction

Nowadays, the development of planar antennas is growing up fast in large number of imaging applications at different wavelengths, from astrophysics [1–3] up to a great variety of civilian markets [4, 5], and especially in the terahertz range due to the emerging generation of wireless communication systems [6]. In the particular case, the detectors based in antenna-coupled bolometers at wavelengths between 8 and 13 μm play an important role because the atmosphere is almost transparent for the incoming electromagnetic radiation and most of the warm objects in the Earth emit radiation in this spectral range.

In general terms, a bolometer is a device for gauging electromagnetic radiation by means of heating of a material with a temperature-dependent electrical resistance. Bolometers are very sensitive to any kind of energy that is deposited in them. They have been used in astronomical instruments with great success in both ground-based and space-borne telescopes [7–9] by using complex and expensive cooling systems that can achieve temperatures between 0.1 K and 0.3 K during their operation. Recent studies [10] demonstrate that bolometers can also be performed at higher temperatures, for example, at 39 K, whose application can be focused towards studies of cold planetary objects in the solar system, and up to temperatures of 93 K for detection of microwave radiation [11], whereas most of civilian applications such as security or defense require uncooled bolometers operating at environment temperatures that can be integrated in compact systems since they must be suitable for mobility [12–14].

A bolometer can be fabricated up to ten times smaller than the desired radiation wavelength to increase its sensitivity and to reduce its time constant. But, in consequence, less energy will be collected because the collected radiation turns to be proportional to the physical size of such bolometer. To overcome this problem, the coupling of planar antennas resonating at the desired wavelength is a good solution to develop fast bolometers without sacrificing collection area. This was demonstrated with various designs for the detection of infrared radiation [15–19].

In this paper we present a model of an antenna-coupled microbolometer for operation in the 30 THz band. Our model consists in a squared pixel structure designed on a 1 μm thick silicon nitride membrane as support frame of 20 μm in

size. A double dipole antenna is joined to microstrip bandpass filters to define the band frequencies, while a load resistance acts as bolometric sensor, and a passive element works as radiation absorber. The model presented here is aimed at being included in focal plane arrays and is exploratory for the field of imaging in astronomy. The model has been simulated using the commercial electromagnetic software HFSS, which is based on the finite elements method.

2. Background Theory

Most of the theories and methods reported in the literature [20–25] for estimating the figures of merit of a bolometer are consistent with each other for any thermal detector and depend upon the characteristics of each design. In general terms, the theory defines the thermal time constant τ, of a bolometer detector as the ratio of heat capacity C to thermal conductance G of the device, that is, by

$$\tau = \frac{C}{G}. \tag{1}$$

The responsivity R_v, as the output voltage per unit of input power, is as follows:

$$R_v = \frac{V_s}{P_i A_d}, \tag{2}$$

where P_i is the intensity of the input power and A_d is the device active area. The detectivity D^*, as the signal to noise ratio with respect to bandwidth Δf and A_d, is as follows:

$$D^* = \frac{(A_d \Delta f)^{1/2}}{\text{NEP}}, \tag{3}$$

where NEP $= V_i/R_v$ is the noise-equivalent power, that is, the incident radiant power required to generate a signal voltage equal to the noise voltage (obtained by dividing the noise voltage by the responsivity) [21].

3. Model of a Single Antenna-Coupled Microbolometer

The geometry of the antenna coupled to a microbolometer is depicted in Figure 1. The antenna, the microstrip feed lines, and the microstrip filters were modeled using 100 nm thick aluminum (Al), considered here as perfect conductor material, whose physical properties are included in the system's library of the software, that is, $\varepsilon_r = 1$, $\sigma = 38 \times 10^6$ siemens/m, and so forth. The length of the metal structure is fixed to 16 μm, whereas the dimensions of the filters and dipoles are varied in order to achieve the desired frequency band (30 THz), which is equivalent to $\lambda = 10\,\mu$m. The microstrip feed lines and filters have 0.25 μm width. The filters are separated 0.5 μm from each other with lengths of 1.75 and 2.5 μm, respectively, and they are placed at each side of the feed lines. The dipole dimensions are proportional to $\lambda/4$ to get optimal antenna efficiency. Each dipole is

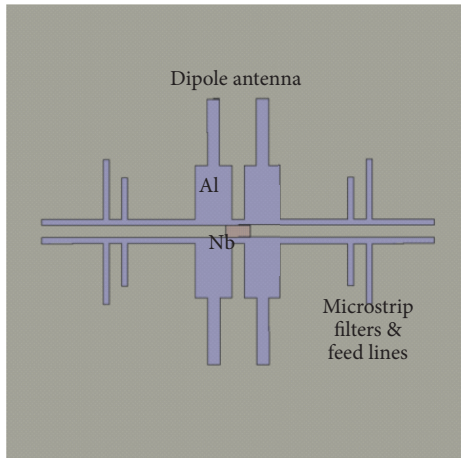

Figure 1: Antenna geometry (not to scale) coupled to a Nb microbolometer. The squared background corresponds to a pixel area of $20 \times 20\,\mu\text{m}^2$.

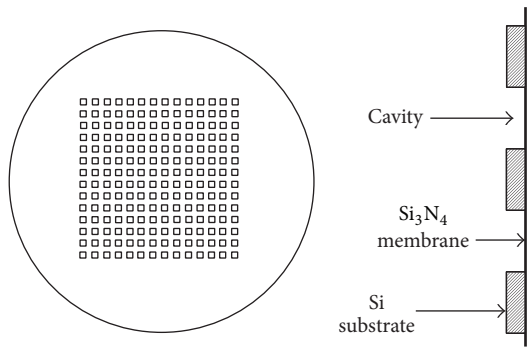

Figure 2: Schematic arrangement (not to scale) for a silicon substrate periodically perforated, with 196 cavities of $1 \times 1\,\mu\text{m}^2$ each one.

composed of a rectangular base of $1.5 \times 2.25\,\mu\text{m}^2$ with a rectangular extension of $0.5 \times 2.75\,\mu\text{m}^2$ thus giving a total length of 5 μm ($\lambda/2$). The microbolometer is modeled with niobium (Nb) of $0.5 \times 1.0 \times 0.1\,\mu\text{m}^3$, and the ground plane acting as an absorber is modeled with 50 nm thick chromium (Cr). The whole structure is suspended on a silicon nitride membrane of $20 \times 20\,\mu\text{m}^2$ and 1 μm thickness. In this model, we propose a membrane suspended on a periodically perforated silicon substrate, as is shown in Figure 2. Here, the proposed substrate has 50.8 mm diameter with 196 cavities of $1 \times 1\,\text{mm}^2$ each one. This kind of membranes can be easily fabricated using standard microelectronic techniques and can also be characterized for use as frequency selective surfaces in astronomical detectors [26].

4. Simulation Results

For a single antenna, the return loss is shown in Figure 3. The antenna exhibits a frequency range of operation at −10 dB

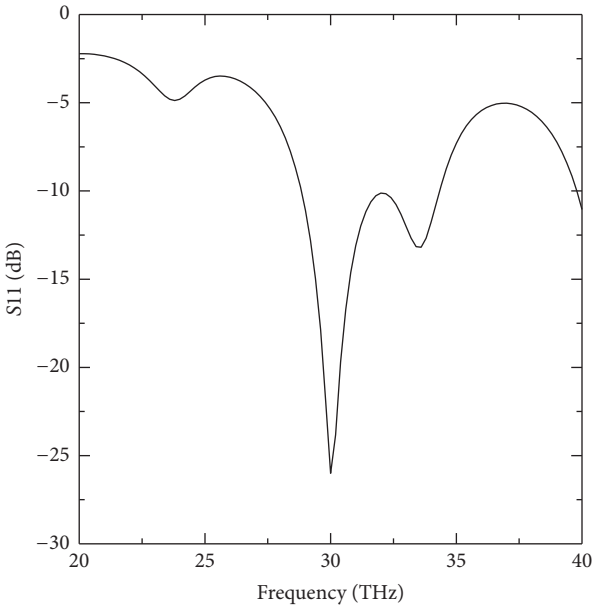

Figure 3: Simulated return loss for a single antenna.

from 27 to 35 THz, which is equivalent to wavelengths $8 < \lambda < 12\,\mu$m, with a narrow bandwidth centered at 30 THz and a second resonance around 34 THz.

In Figure 4, the gain patterns are presented for a single antenna, for an array of 10×10 elements, and for an array of 50×50 elements, respectively. Note that in this simulation for the array of 10×10 elements the beam pattern of the main lobe and the side lobes show high degree of symmetry for both the *E-H* planes. It is also observed that, by increasing the number of antenna elements in an array of $N \times N$, the half power beamwidth (HPBW) is reduced down approximately by a factor of N, while the gain (G) increases proportionally to N. That is easy to observe since for a single antenna we have a HPBW $\sim 25^\circ$ with the first side lobes relative to the maximum at $G \sim 0.5$ dB; for an array of 10×10 elements we have a HPBW $\sim 2.5^\circ$ with the first side lobes at $G \sim 0.8$ dB; and for an array of 50×50 elements we have a HPBW $\sim 0.5^\circ$ with the first side lobes at $G \sim 0.85$ dB, respectively. A summary of the parameters obtained by simulation for a single antenna is shown in Figure 5.

Each cavity of $1\,\text{mm}^2$ in the proposed substrate can hold an array of 50×50 antenna structures that can be connected in a series-parallel combination. For this particular case, each array will provide a single pixel with much higher directivity and a dc resistance approximately the same as that of a single antenna. Hence, we will have a two-dimensional array of 196 pixels in a squared area of $27 \times 27\,\text{mm}^2$.

On the other hand, the analytical predictions for our detector are based on the bolometer's theory, which indicates that one of the most important factors that affect its performance is the thermal conductance G, which is essential for determining the time constant. However, it is not easy to predict with accuracy since it involves several factors that can only be determined experimentally; for instance, one way for estimating G is by heating the bolometer by bias current only and measuring the bolometer resistance; then G can be calculated from a relation between the inverse of resistance measured in the bolometer and the square of the applied bias current, whereas the heat capacity can be calculated as $C = V\rho c$, where V is the volume of the detector determined from the design and ρ and c are the density and specific heat, respectively. For different materials, C can be found in tables and in the literature [22]; hence, for our design the heat capacity can be established as $C = 11.6 \times 10^{-14}$ J/K and G as a typical value of order of $G = 2 \times 10^{-5}$ W/K. Therefore, the time constant according to (1) provides a value of $\tau = 5.8$ ns.

Referring to parameters obtained in Figure 5, the device active area A_d is related to the maximum directivity of the antenna [27] by $A_d = \lambda^2 D_{\max}/4\pi = 53.69\,\mu\text{m}^2$.

For estimating the responsivity R_v of our bolometer, we know that the resistivity ρ of niobium at room temperature is $1.44 \times 10^{-6}\,\Omega\cdot$m; then by assuming a typical bias current of $1\,\mu$A, we get an output voltage $V_s = 0.288\,\mu$V. Therefore, according to (2), we have $R_v = 5.3 \times 10^3$ V/W.

Finally, from (3), the NEP can be determined by calculating the *Johnson noise* whose voltage is given by $V_J = (4kT_dR_e\Delta f)^{1/2}$ [22], where k is the Boltzmann's constant, T_d is the absolute temperature of the bolometer, and R_e is the resistance of the bolometer, thus giving a result of $V_J = 1.95 \times 10^{-4}$ V, and NEP $= 3.7 \times 10^{-8}$ W. Therefore, the estimated detectivity will be of order of $D^* = 2.07 \times 10^{10}\,\text{cm}\sqrt{\text{Hz}}/\text{W}$. It should be pointed out that the simulations and the predicted values shown here were made considering room temperature and vacuum conditions; therefore the heat transfer caused by convection and radiation were not taken into account. It is not surprising to get D^* of order of 10^{10}; another model using different software has been reported before with estimated values of order of 10^9 [28]. For the case when we considered air atmosphere only, then the detectivity could turn to be of order of $D^* = 1 \times 10^7\,\text{cm}\sqrt{\text{Hz}}/\text{W}$.

5. Conclusions

In this paper, a model of an antenna-coupled microbolometer has been presented. The figures of merit have been predicted analytically. The characteristics and radiation patterns of the antenna were simulated using a commercial electromagnetic package. The results reveal feasibility for integration in focal plane arrays. The presented design is the first step towards the development of multiple arrays to study their feasibility and use in astronomical applications; even for this, the device requires vacuum and cryogenic environments for its operation. This turns to be a challenge for us, since the state of the art of astronomical instruments at LWIR frequencies still is not widely explored.

Future work will consist in building these designs on periodically perforated silicon substrates. The use of new modeling methods for getting accurate characterization [29] will be considered.

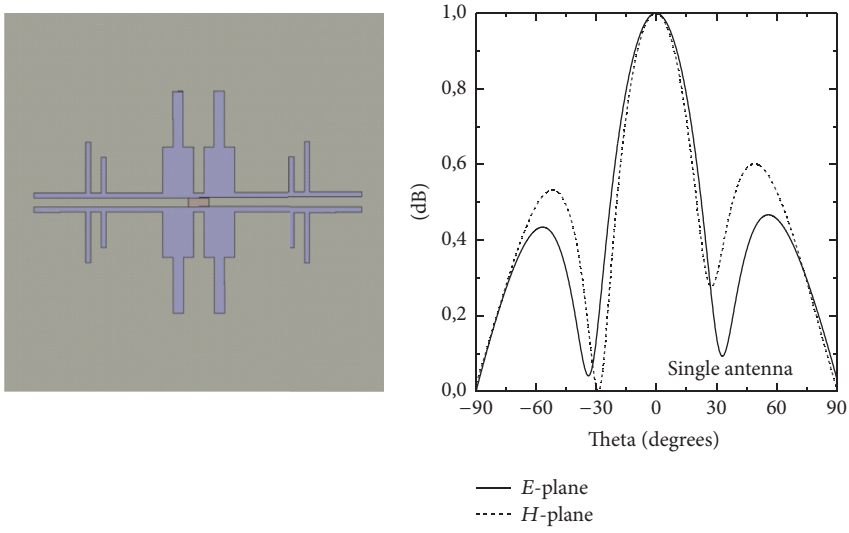

(a)

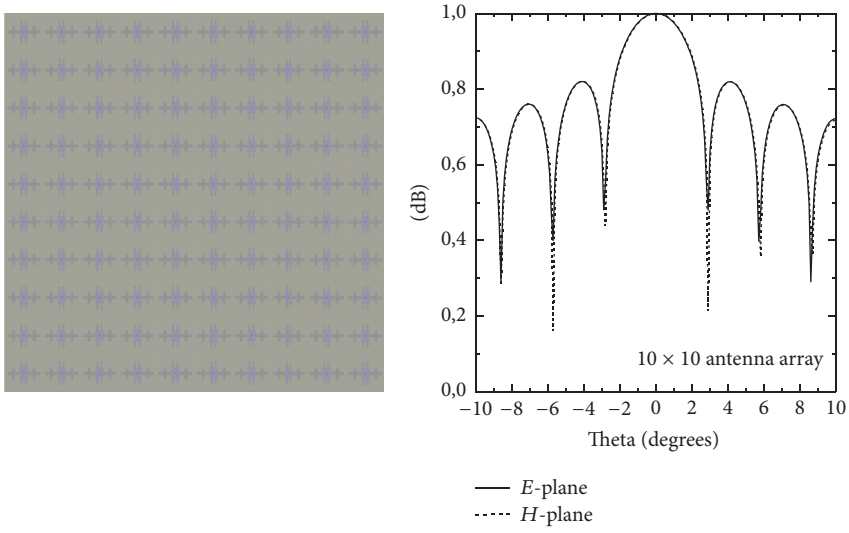

(b)

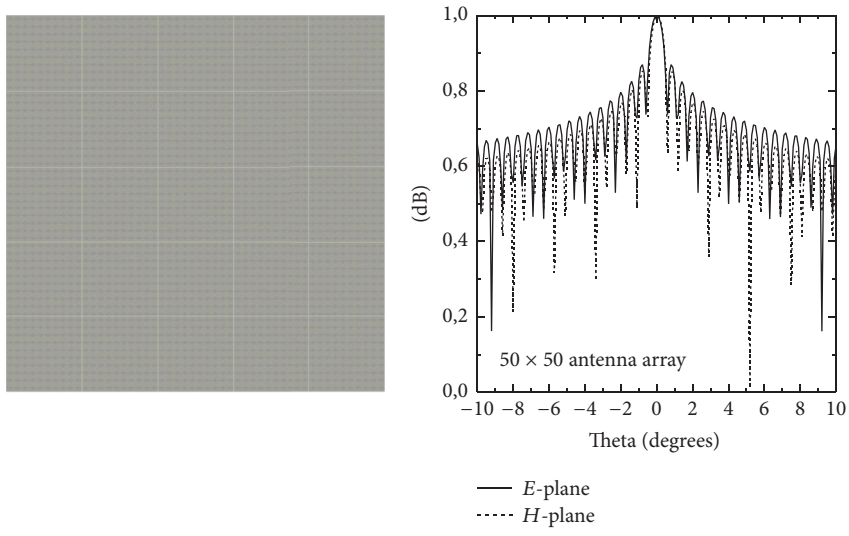

(c)

Figure 4: Gain patterns relative to the maximum for a single antenna, for an array of 10×10 elements, and for an array of 50×50 elements. The squared backgrounds correspond to pixel areas of $20 \times 20\,\mu m^2$ (a), $200 \times 200\,\mu m^2$ (b), and $1000 \times 1000\,\mu m^2$ (c), respectively.

Antenna Parameters:

	Quantity	Value	Units
	Max U	0.064174	W/sr
	Peak Directivity	6.7467	
	Peak Gain	0.80848	
	Peak Realized Gain	0.80645	
	Radiated Power	0.11953	W
	Accepted Power	0.99749	W
	Incident Power	1	W
	Radiation Efficiency	0.11983	
	Front to Back Ratio	1.#INF	
	Decay Factor	0	

Maximum Field Data:

	rE Field	Value	Units	At Phi	At Theta
	Total	6.9561	V	90deg	-0.29999...
	X	6.9548	V	90deg	-0.29999...
	Y	0.18493	V	0deg	-25deg
	Z	2.5198	V	0deg	61.2deg
	Phi	6.9548	V	90deg	-0.29999...
	Theta	6.9541	V	0deg	-0.19999...
	LHCP	5.0114	V	90deg	-0.39999...
	RHCP	4.8244	V	90deg	-0.19999...
	Ludwig3/X dominant	6.9548	V	90deg	-0.29999...
	Ludwig3/Y dominant	0.18493	V	0deg	-25deg

Figure 5: Antenna parameters obtained by simulation.

Conflicts of Interest

The authors declare that there are no conflicts of interest regarding the publication of this paper.

Acknowledgments

This project is supported by Agencia Espacial Mexicana (AEM), through a Grant no. AEM-2014-1-248438.

References

[1] A. Colin, D. Ortiz, E. Villa, E. Artal, and E. Martínez-González, "An array of lens-coupled antennas for cosmic microwave background measurements in the 30 Ghz band," *Experimental Astronomy*, vol. 33, no. 1, pp. 27–37, 2012.

[2] M. J. Myers, K. Arnold, P. Ade et al., "Antenna-coupled bolometer arrays for measurement of the cosmic microwave background polarization," *Journal of Low Temperature Physics*, vol. 151, no. 1-2, pp. 464–470, 2008.

[3] A. Baryshev, J. J. A. Baselmans, A. Freni et al., "Progress in antenna coupled kinetic inductance detectors," *IEEE Transactions on Terahertz Science and Technology*, vol. 1, no. 1, pp. 112–123, 2011.

[4] F. J. González, B. Ilic, J. Alda, and G. D. Boreman, "Antenna-coupled infrared detectors for imaging applications," *IEEE Journal on Selected Topics in Quantum Electronics*, vol. 11, no. 1, pp. 117–120, 2005.

[5] W. Yang, M. C. Roggemann, K. Cooper et al., "The IR antenna pair coupled sensor element and its potential application in wavefront sensing," *Infrared Physics and Technology*, vol. 51, no. 6, pp. 495–504, 2008.

[6] K. R. Jha and G. Singh, "Terahertz planar antennas for future wireless communication: A technical review," *Infrared Physics and Technology*, vol. 60, pp. 71–80, 2013.

[7] G. Siringo, E. Kreysa, A. Kovács et al., "The large APEX BOlometer CAmera LABOCA," *Astronomy and Astrophysics*, vol. 497, no. 3, pp. 945–962, 2009.

[8] J. A. Tauber, N. Mandolesi, J.-L. Puget et al., "Planck pre-launch status: the Planck mission," *Astronomy and Astrophysics*, vol. 520, no. 1, article A1, 2010.

[9] A. Poglitsch, C. Waelkens, N. Geis et al., "The Photodetector Array Camera and Spectrometer (PACS) on the herschel space observatory," *Astronomy and Astrophysics*, vol. 518, article L2, 2010.

[10] B. Lakew, S. Aslam, J. Brasunas et al., "MgB2 thin-film bolometer for applications in far-infrared instruments on future planetary missions," *Physica C: Superconductivity and its Applications*, vol. 483, pp. 119–126, 2012.

[11] S. F. Karmanenko, A. A. Semenov, I. A. Khrebtov et al., "Fabrication process and noise properties of antenna-coupled microbolometers based on superconducting YBCO films," *Superconductor Science and Technology*, vol. 13, no. 3, pp. 273–286, 2000.

[12] U. Mizrahi, F. Schapiro, L. Bykov et al., "Advanced μ-bolometer detectors for high-end applications," in *Infrared Technology and Applications XXXVIII*, vol. 8353 of *Proceedings of SPIE*, Baltimore, Md, USA, April 2012.

[13] J. LaVeigne, G. Franks, K. Sparkman, M. Prewarski, B. Nehring, and S. McHugh, "LWIR NUC using an uncooled microbolometer camera," in *Technologies for Synthetic Environments: Hardware-in-the-Loop Testing XV*, vol. 7663 of *Proceedings of SPIE*, Orlando, Fla, USA, April 2010.

[14] J. Lee, C. Rodriguez, and R. Blackwell, "BAE Systems' 17μm LWIR camera core for civil, commercial and military applications," in *Infrared Technology and Applications XXXIX*, vol. 8704 of *Proceedings of SPIE*, Baltimore, Md, USA, May 2013.

[15] D. P. Neikirk, W. W. Lam, and D. B. Rutledge, "Far-infrared microbolometer detectors," *International Journal of Infrared and Millimeter Waves*, vol. 5, no. 3, pp. 245–278, 1984.

[16] I. Wilke, W. Herrmann, and F. K. Kneubühl, "Integrated nanostrip dipole antennas for coherent 30 THz infrared radiation," *Applied Physics B Laser and Optics*, vol. 58, no. 2, pp. 87–95, 1994.

[17] I. Codreanu, C. Fumeaux, D. F. Spencer, and G. D. Boreman, "Microstrip antenna-coupled infrared detector," *Electronics Letters*, vol. 35, no. 25, pp. 2166-2167, 1999.

[18] F. J. González and G. D. Boreman, "Comparison of dipole, bowtie, spiral and log-periodic IR antennas," *Infrared Physics & Technology*, vol. 46, no. 5, pp. 418–428, 2005.

[19] F. J. González, B. Ilic, and G. D. Boreman, "Antenna-coupled microbolometers on a silicon-nitride membrane," *Microwave and Optical Technology Letters*, vol. 47, no. 6, pp. 546–548, 2005.

[20] P. W. Kruse, L. D. McGlauchlin, and R. B. McQuistan, *Elements of infrared technology*, John Wiley and Sons, 1962.

[21] P. W. Kruse, "Physics and applications of high-Tc superconductors for infrared detectors," *Semiconductor Science and Technology*, vol. 5, no. 3 S, article no. 051, pp. S229–S239, 1990.

[22] P. Eriksson, J. Y. Andersson, and G. Stemme, "Thermal characterization of surface-micromachined silicon nitride membranes for thermal infrared detectors," *Journal of Microelectromechanical Systems*, vol. 6, no. 1, pp. 55–61, 1997.

[23] F. J. González, M. A. Gritz, C. Fumeaux, and G. D. Boreman, "Two dimensional array of antenna-coupled microbolometers," *International Journal of Infrared and Millimeter Waves*, vol. 23, no. 5, pp. 785–797, 2002.

[24] J. D. Vincent, *Fundamentals of Infrared Detector Operation and Testing*, John Wiley and Sons, 1990.

[25] A. Rogalski, *Infrared Detectors*, CRC Press, 2010.

[26] A. Colin, "Characterization of a sub-mm wave fre- quency selective surface on a periodically perforated silicon substrate," *Progress In Electromagnetics Research M*, vol. 27, pp. 75–81, 2012.

[27] C. A. Balanis, *Antenna Theory*, John Wiley and Sons, New York, NY, USA, 1997.

[28] F. J. González, "Themal impedance sumulations of antenna-coupled microbolometers," *Infrared Physics & Technology*, vol. 48, pp. 223–226, 2006.

[29] J. Ginn, B. Lail, D. Shelton, J. Tharp, W. Folks, and G. Boreman, "Characterizing infrared frequency selective surfaces on dispersive media," *Applied Computational Electromagnetics Society Journal*, vol. 22, no. 1, pp. 184–188, 2007.